THE JOURNAL OF COMPARATIVE NEUROLOGY 481:6–18 (2005)

Avian Superior Olivary Nucleus Provides Divergent Inhibitory Input to Parallel Auditory Pathways

R. MICHAEL BURGER, KARINA S. CRAMER, JOSHUA D. PFEIFFER, AND EDWIN W RUBEL*
Virginia Merrill Bloedel Hearing Research Center and Department of Otolaryngology–Head and Neck Surgery, University of Washington, Seattle, Washington 98195-7923

ABSTRACT

The avian auditory brainstem displays parallel processing, a fundamental feature of vertebrate sensory systems. Nuclei specialized for temporal processing are largely separate from those processing other aspects of sound. One possible exception to this parallel organization is the inhibitory input provided by the superior olivary nucleus (SON) to nucleus angularis (NA), nucleus magnocellularis (NM), and nucleus laminaris (NL) and contralateral SON (SONc). We sought to determine whether single SON neurons project to multiple targets or separate neuronal populations project independently to individual target nuclei. We introduced two different fluorescent tracer molecules into pairs of target nuclei and quantified the extent to which retrogradely labeled SON neurons were double labeled. A large proportion of double-labeled SON somata were observed in all cases in which injections were made into any pair of ipsilateral targets (NA and NM, NA and NL, or NM and NL), suggesting that many individual SON neurons project to multiple targets. In contrast, when injections involved the SONc and any or all of the ipsilateral targets, double labeling was rare, suggesting that contralateral and ipsilateral targets are innervated by distinct populations of SON neurons arising largely from regionally segregated areas of SON. Therefore, at the earliest stages of auditory processing, there is interaction between pathways specialized to process temporal cues and those that process other acoustic features. We present a conceptual model that incorporates these results and suggest that SON circuitry, in part, functions to offset interaural intensity differences in interaural time difference processing. J. Comp. Neurol. 481:6–18, 2005.

Indexing terms: binaural; GABA; topography; interaural time disparity; sound localization; electroporation

A hallmark of sensory processing is the presence of parallel pathways for computation of various features of environmental signals. In the avian auditory brainstem, these pathways originate in auditory nerve axons as they bifurcate to innervate nucleus magnocellularis (NM) and nucleus angularis (NA; Boord and Rasmussen, 1963; Ramon y Cajal, 1908; Parks and Rubel, 1978). This divergence initiates two parallel pathways that ascend the auditory system. One, originating in nucleus magnocellularis (NM), is clearly specialized for computing temporal aspects of the signal (Parks and Rubel, 1975; Young and Rubel, 1983; Sullivan and Konishi, 1984; Köppl, 1997; Trussell, 1999; Monsivais et al., 2000). The other, originating in NA, likely processes multiple features of the signal (Hotta, 1971; Sullivan and Konishi, 1984; Warchol and Dallos, 1990; Soares and Carr, 2001; Soares et al., 2002; Köppl and Carr, 2003). The avian brainstem audi-

Grant sponsor: National Institute on Deafness and Other Communication Disorders; Grant number: DC00395; Grant number: DC04661; Grant number: DC00466.

Dr. Cramer's present address is Department of Neurobiology and Behavior, University of California, Irvine, California 92697.

*Correspondence to: Edwin W Rubel, Virginia Merrill Bloedel Hearing Research Center and Department of Otolaryngology-HNS, Box 357923, University of Washington, Seattle WA 98195-7923.
E-mail: rubel@u.washington.edu

Received 14 May 2004; Revised 21 July 2004; Accepted 26 August 2004
DOI 10.1002/cne.20334
Published online in Wiley InterScience (www.interscience.wiley.com).

tory system includes two additional nuclei. The first, nucleus laminaris (NL), is the target of bilateral excitatory input from NM and is devoted to processing interaural time differences (ITDs; Parks and Rubel, 1975; Rubel and Parks, 1975; Young and Rubel, 1983; Carr and Konishi, 1990; Pena et al., 1996; Viete et al., 1997). The second, the superior olivary nucleus (SON), contains predominantly γ-aminobutyric acid (GABA)ergic neurons and communicates with both ascending pathways (Lachica et al., 1994; Westerberg and Schwarz, 1995; Yang et al., 1999; Monsivais et al., 2000).

In addition to innervating different target nuclei in the lateral lemniscus and largely separate regions of the midbrain nucleus mesencephalicus lateralis pars dorsalis (MLd), the outputs of NA and NL both converge on the SON (Conlee and Parks, 1986; Takahashi and Konishi, 1988). The SON, in turn, projects back ipsilaterally to all three lower nuclei NA, NM, and NL and to the contralateral SON (SONc; Conlee and Parks, 1986; Monsivais et al., 2000). Considerable attention has been devoted to the cellular physiology of the SON projection onto NM and NL, but little is known about the precise nature of the anatomical organization of this projection (Funabiki et al., 1998; Yang et al., 1999; Lu and Trussell, 2000, 2001; Monsivais et al., 2000; Monsivais and Rubel, 2001). Understanding this anatomy is critical for predicting its role(s) in auditory processing. A few of many possible output patterns to lower order brainstem nuclei are illustrated in Figure 1.

This study was initiated to determine the degree of segregation of ascending pathways as modified by their connections with SON. Additionally, we assessed the topographic organization of the SON projections back to NM and NL, where the tonotopic axis has been described in detail. We used an in vitro retrograde labeling method to identify populations of SON neurons that project to NA, NM, and NL, as well as the SONc. The results indicate that most SON neurons project to two or more ipsilateral targets: NA and NM, NA and NL, or NM and NL. Additionally, separate populations of SON neurons innervate ipsilateral and contralateral targets, suggesting independent regulation of ascending and descending inhibition in the brainstem auditory system.

MATERIALS AND METHODS

In vitro preparation

Twenty-nine white Leghorn chicken embryos, ages embryonic day (E) 18–21, were used to provide the final data reported here. A larger number were used to develop the methods. At these ages, the chicken auditory system is known to be mature (Rubel, 1978). All procedures involving animals in this study followed protocols approved by University of Washington's Institutional Animal Care and Use Committee and conformed to National Institutes of Health guidelines. An in vitro preparation adapted from (Hackett et al., 1982) was used to facilitate labeling of target nuclei. Briefly, embryos were partially extracted from their shells and rapidly decapitated. The skull was sectioned at the level of the brainstem and the resulting tissue was submerged in oxygenated Tyrode's solution (in mM: 140 NaCl, 2.9 KCl, 17 $NaHCO_3$, 0.1 $MgCl_2$, 1.8 $CaCl_2$, 120 glucose in dH_2O) in a Sylguard-coated Petri dish at 22°C. The brainstem was carefully dissected away

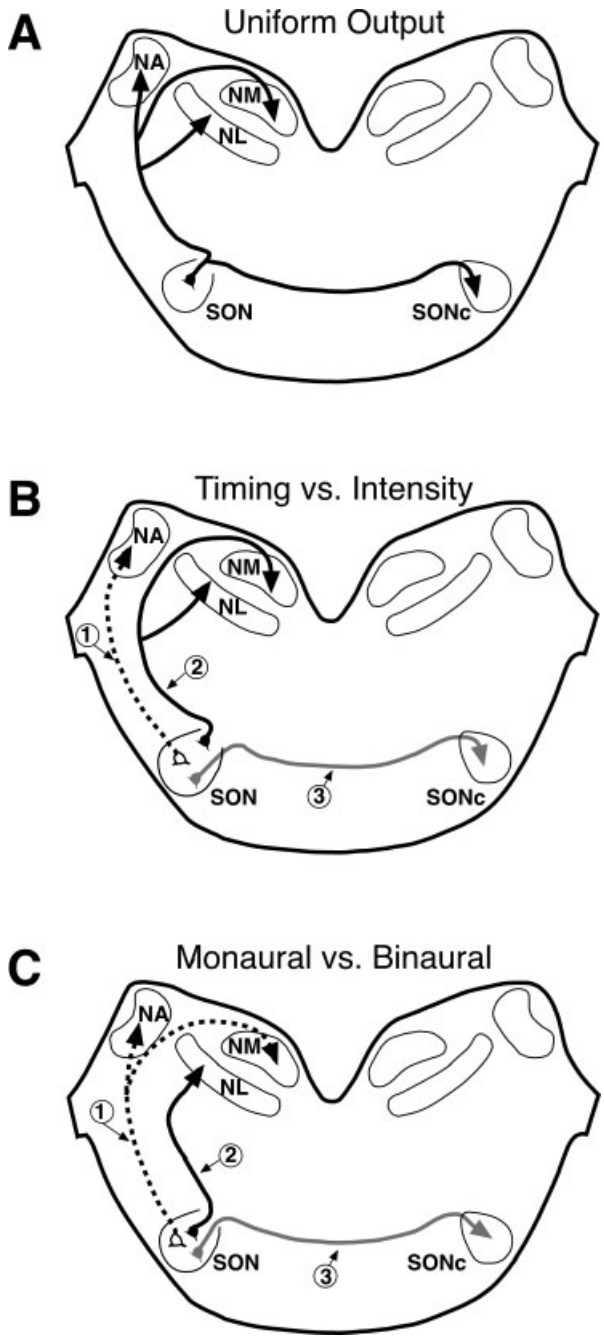

Fig. 1. Schematic diagrams outlining some of the many possible output patterns of the superior olivary nucleus (SON). Populations of SON neurons are represented as individual somata with projections emanating from the SON at left. **A:** A single SON population projecting to all of its known brainstem targets black solid lines. NA, nucleus angularis; NM, nucleus magnocellularis; NL, nucleus laminaris; SONc, contralateral SON. **B:** Three separate populations projecting to different sets of targets, preserving the parallel pathways established in the cochlear nuclei: (1) NA, dashed line; (2) NM and NL ("timing pathway" targets), solid black line; and (3) SONc, solid gray line. **C:** An alternative set of three projections targeting (1) monaural targets in NA and NM (dashed line), (2) the binaural target NL (solid black line), and (3) SONc (solid gray line).

from the surrounding tissue, and the cerebellum was removed at the peduncles. With the brainstem dissected free and maintained with oxygenated Tyrode's solution, the locations of NM, NL, and NA could be determined relative to the visible course of the myelinated auditory nerve over the surface of the brainstem. This visualization greatly facilitated targeting of NM, NL, and NA for injection.

In vitro electroporation

Previous studies using traditional retrograde labeling methods have reported that SON neurons are resistant to labeling (Correia et al., 1982; von Bartheld and Rubel, 1989). Our initial experiments using iontophoresis or pressure injections of fluorescently tagged dextrans confirmed these difficulties. By using these methods, however, we observed excellent retrograde labeling of the contralateral NM, indicating that the tissue was healthy, but we seldom obtained satisfactory labeling of SON neurons. We overcame this difficulty by adapting a labeling method that used dye electroporation to augment dye delivery and uptake (Neumann et al., 1999; Haas et al., 2002). This method greatly enhanced retrograde labeling of SON neurons.

Tracers were delivered through pulled glass pipettes (A-M Systems, Carlsbourg, WA) with tip diameters of 5–10 μm. The pipette was advanced into the target nuclei under visual control using a Leica MZFLIII (Leica, Inc., Northvale, NJ) fluorescent dissecting microscope. Retrograde tracer solutions contained 6.25% 3,000 molecular weight tetramethylrhodamine dextran (RDA; Molecular Probes, Eugene, OR) or 10% 10,000 molecular weight Alexa 488 dextran (Alexa488DA; Molecular Probes) in phosphate buffered saline (PBS), pH 7.4 containing 0.4% Triton X-100. Tracers were applied by pressure pulses of 20–50 msec at ~10 pounds per square inch delivered by a Picospritzer (General Valve Corporation, E. Hanover, NJ). Concurrent with or immediately after pressure pulses, electroporation voltage steps were delivered through an Electro Square Porator (BTX model ECM 830, San Diego, CA). Voltage steps were typically three sets of eight-pulse trains at 50 V and 50-msec duration at 10 Hz. The dye pipette served as the cathode through a silver wire inserted into the pipette and the bath solution was coupled to the anode. After injection and electroporation, brainstems were transferred to a chamber containing continually oxygenated Tyrode's solution for 4–6 hours at 22°C then transferred individually to separate sealed 50-ml containers of oxygenated Tyrode's overnight at 4°C . The tissue was then fixed in 4% paraformaldehyde in PBS for 4–5 hours, followed by several rinses in PBS, then cryoprotected in a solution of 30% sucrose in PBS overnight. Brainstems were blocked and embedded in Tissue Tek OCT (Sakura Finetek, Torrance, CA) at −20°C and sectioned in the coronal plane at 14 μm on a cryostat.

Imaging and reconstruction

Sections were viewed on a Nikon (Melville, NY) EFD-3 fluorescent microscope fitted with filter cubes to isolate the two fluorophores. In several cases, images were taken using the opposing filter at singly labeled injection sites to rule out signal bleed between channels. Monochrome images were taken of each section containing the SON at high magnification in each of the two channels with a Spot 1.4.0 camera (Diagnostic Instruments, Sterling Heights, MI). Additionally, in many cases, a darkfield image was acquired of each section through SON and the injection sites. These images facilitated identification of nuclear borders and landmarks (see Fig. 3, for example).

After imaging, the neurons labeled with each fluorophore were separately counted in each section through the SON. The two channels were then merged, and the dynamic ranges of pixel values for both channels were normalized to each other in Adobe Photoshop 5.5 (Adobe Systems, Inc., Seattle, WA). Neurons were identified by viewing each channel independently and marking cells that had completely filled somata with labeling levels that were above background. Neurons meeting these criteria in both channels were deemed to be double labeled. For preparations involving injections of two separate fluorophores, the percentage of double-labeled cells reported here is defined as the number of double-labeled cells expressed as a percentage of the lower number of labeled cells counted in either of the two channels. For example, if 50 cells were double labeled in a population where 100 cells were RDA-positive and 500 were Alexa488DA-positive, the percentage reported would be 50%. By reporting double labeling in this way, we adjusted for the proportion of the total population of labeled cells that was available for double labeling.

Topographic studies

The topographic distributions of SON neurons were studied for several conditions described in the Results section. Injection site borders were operationally defined by the coalesced appearance of nonspecific labeling (i.e., labeling not associated with cellular structures) in the neuropil. Serial images through the entire SON were imported into Freehand (Macromedia, Inc., San Francisco, CA) graphics software. The coordinate locations of each SON neuron were then marked within its borders. The reconstructed SON volume was then divided into eight divisions by bisecting the three cardinal dimensions of SON. Cell counts were then made for each octant division, and distributions of neurons generated by various injection locations were analyzed.

RESULTS

Evaluation of labeling methods

We tested several dye delivery methods, including pressure alone, iontophoresis alone, and pressure combined with either iontophoresis or electroporation. Pressure pulses coupled with electroporation into NA, NM, or NL typically resulted in hundreds of SON neurons labeled. This finding is in contrast to pressure ($n = 4$), iontophoretic ($n = 5$), or pressure and iontophoretic in combination ($n = 18$) approaches that usually yielded retrograde labeling in several areas, including the contralateral NM, but rarely yielded any retrogradely labeled somata in SON. These methods did orthogradely label the axons projecting from NA and NL to SON (data not shown).

The primary goal of this study was to determine whether individual SON neurons project to multiple targets in the auditory brainstem. A potential difficulty with the method we used is that the two dextrans may be taken up for retrograde labeling with different efficiency, thus influencing our quantification of double labeling. Therefore, to study the efficiency of double labeling, in five preparations, the two solutions were mixed 1:1 by volume

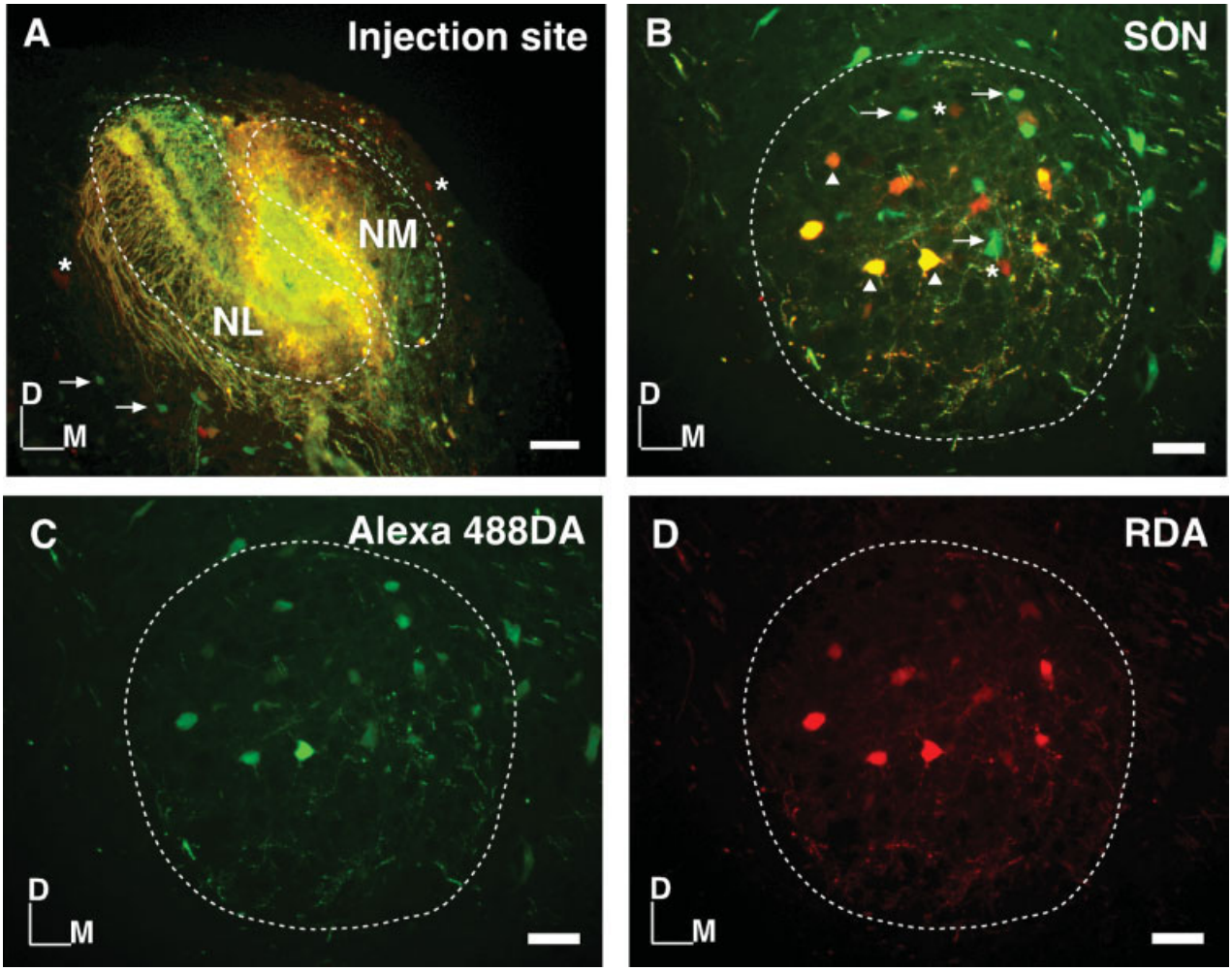

Fig. 2. Double labeling does not reach 100% when dyes are mixed. **A:** An injection of a mixture of tetramethylrhodamine dextran (RDA) and Alexa488DA that appears yellow due to the near complete overlap of dyes. The injection site is centered between nucleus magnocellularis (NM) and nucleus laminaris (NL) and encroaches on both nuclei. Labeled somata close to the injection site show a bias for either green (arrows) or red (asterisks) dextrans. **B:** A section through superior olivary nucleus (SON). Numerous cells are double labeled (arrowheads), appearing yellow or orange. There are also singly labeled neurons in the field (arrows and asterisks). **C,D:** Images of the individual labels for the merged image shown in B. Orientation bars in lower left of each panel indicate dorsal (D) and medial (M) directions. Scale bars = 100 μm in A; 50μm in B–D.

before injection into target nuclei. Assuming equivalent efficiency uptake and transport of each label, one would predict that 100% of retrogradely labeled SON neurons would be double labeled. Alternatively, if there are differences in uptake between the dyes, one might expect 100% of the cells labeled with the less-efficient dye would be double labeled. Neither of these alternative scenarios proved true. In most cases, many singly labeled SON neurons were present. On average 83.4% (see Materials and Methods section for calculation of percentage double label) of the neurons in SON that showed any label were double labeled when a 1:1 mixture of both fluorophores was injected into a single target location. A representative case is shown in Figure 2. Figure 2A shows the near complete overlap of the two labels at the injection site that covers medial NL and ventral NM. Figure 2B shows the resulting labeling pattern in the ipsilateral SON. Most cells are double labeled and appear yellow (Figure 2B, arrowheads). However, several somata only had detectable label in either the green (Figure 2B, arrows) or red (Figure 2B, asterisks) channel. For reference, the images of each channel alone are presented in Figure 2C,D. In the five brainstems tested with mixed dye injections, the range in the proportion of double-labeled SON neurons was 69.9–98.9%. Across the population there was no systematic bias in the efficacy of the two labels, all data appear in Table 1. Because double labeling was not observed in 100% of the somata when the dyes are equally mixed before injection, the proportion of all neurons observed to be double labeled in subsequent experiments should be considered conservative.

SON projections to multiple ipsilateral targets

The principal issue addressed in this report is whether SON projections to each of its brainstem target nuclei

TABLE 1. Double Labeling of SON Somata From Multiple Targets[1]

Case	RDA (target nucleus)	Alexa488DA (target nucleus)	# Double	% Double
NA plus NL				
015102C	379 (NL)	249 (NA)	33	13.3
015102A	299 (NA)	102 (NL)	20	19.6
015105E	296 (NA)	102 (NL)	2	2
015101D	280 (NA)	250 (NL)	82	32.8
015103B	103 (NL)	105 (NA)	5	4.9
Average				**14.5**
NA plus NM/NL				
025101C	54 (NA)	261 (NM/NL)	3	5.6
025103C	270 (NA)	120 (NM/NL)	46	38.3
025101B	467 (NM/NL)	157 (NA)	43	27.3
Average				**23.7**
NA plus NM				
015102B	166 (NA)	21 (NM)	4	19.0
025114A	69 (NM)	406 (NA)	8	11.6
025114c	111 (NM)	308 (NA)	15	13.5
Average				**14.7**
NM plus NL				
025108E	153 (NL)	179 (NM)	132	86.3
025113B	120 (NM)	497 (NL)	5	4.2
025113A	78 (NM)	518 (NL)	2	2.6
Average				**31.0**
Mixed dye controls				
025108B	256 (all*)	228	183	80.3
025108A	296 (NM/NL)	387	207	69.9
025104G	196 (all*)	282	187	95.4
025104H	186 (all*)	189	184	98.9
025104I	132 (NM/NL)	133	98	72.4
Average				**83.4**

[1]Results of differential labeling from ipsilateral target nuclei. Each combination category of target nuclei is shown in bold at left. The number and letter combinations *at left* are designations that identify each preparation. The number of cells labeled by each dye is shown in the middle columns, and the target nucleus is shown in parentheses. The percentage of somata that were double labeled (see Materials and Methods section) are shown at the right with the mean for each group in bold at the end of each section. Asterisks indicate injection in each of nucleus angularis (NA), nucleus magnocellularis (NM), and nucleus laminaris (NL).

originate in separate populations of SON neurons with unique targets or whether a single population provides input to all targets. To investigate this question, we delivered different fluorescent dextrans into pairs of target nuclei in the brainstem and evaluated the extent to which SON neurons were labeled with both fluorophores. Double labeling is an indication that a given neuron projects to both injection sites.

In five preparations, one injection was restricted to NA and the other was restricted to NL. In all cases, an abundance of double-labeled cells were observed in SON. Figure 3 shows one case where RDA was injected into NA and Alexa488DA was injected into the ventromedial NL. Figure 3A,B shows the injection sites at two different rostrocaudal levels of these nuclei; Figure 3A is more rostral. Figure 3C shows the ipsilateral SON, with several double-labeled cells indicated by arrowheads. The SON in this embryo had a total of 280 RDA-labeled cells, 250 Alexa488DA-labeled cells, and 82 double-labeled cells; thus, the percentage of double-labeled cells for this embryo was 33%. The mean for this group was 15%. The data for all injections involving pairs of ipsilateral targets is summarized in Table 1.

Figure 4 shows a preparation in which injections covered most of NA (RDA) and a large extent of the ventral and caudal portion of NM (Alexa488DA). Some of the Alexa488DA crossed into the dorsal margin of NL. Figure 4A shows projections of the injection sites at two rostrocaudal levels. Figure 4B shows a photomicrograph of one 14 μm section of the SON with several double-labeled neurons (Figure 4B, arrowheads) along with a few RDA and Alexa488DA singly labeled somata. In this embryo, 38% of labeled SON somata were double labeled, a similar value to the case shown in Figure 3. Nucleus angularis was the target of one of the two injections in five other cases where the opposing injection involved parts of either NM alone or both NM and NL. In all cases, double labeling was observed in SON. The mean proportion of double-labeled somata was 23.7% for NA plus NM/NL injections and 14.7% for NA plus NM injections. In three additional cases, we labeled NM and NL differentially with minimal overlap. This group included one case with the highest overall proportion of double-labeled SON cells at 86.3% as well as two cases with small numbers of double-labeled cells (see Table 1). The average for this group was 31%.

We did not observe labeled somas in the SONc for any injection in NM, NL, or NA. These data taken together, with the caveat from mixed dye injections that double-labeling percentages are likely to be an underestimate of the total population of multi-target SON neurons, suggest that a substantial population of SON neurons projects to two or more ipsilateral targets in the NA, NM, and NL.

SON's contralateral projection is a separate population

The SON is known to project to the SONc and LLv and bilaterally to the MLd as well as its ipsilateral targets in the lower nuclei NL, NM, and NA (Conlee and Parks, 1986; Carr et al., 1989; Lachica et al., 1994; Yang et al., 1999). Because the data presented thus far indicate that many individual neurons in the SON project to multiple ipsilateral targets in its descending projection, we sought to address the question of whether the same population of SON neurons also projects to contralateral targets in the SONc and in higher order nuclei. To address this question, we made several injections of Alexa488DA in the ipsilateral NM, NA, and NL in the same brains as large injections of RDA in the contralateral brainstem within or near the SONc.

In six cases where both the ipsilaterally and contralaterally projecting SON neurons were labeled, double labeling of SON neurons was exceedingly rare, with a mean percent double labeling of 1.5%. Table 2 shows the numbers of cells labeled with each dye corresponding to contralateral or ipsilateral injection sites. One such case is illustrated in Figure 5. Figure 5A shows a composite of the ipsilateral and the contralateral injection fields with the rostrocaudal dimension projected onto the two dimensional coronal drawing. Figure 5B shows a 14 μm section through SON with many RDA (Figure 5B, arrows) and Alexa488DA (Figure 5B, asterisks) -labeled cells but no double labeling. These SON neurons that project to either ipsilateral or contralateral targets appear to be intermingled throughout the nucleus (but see following section). In addition to the paucity of double-labeled SON neurons, the main fiber tract out of SON (Figure 5B, arrowheads) also shows no double labeling in the axons. This lack of double labeling across all six preparations was striking, considering the high number of neurons that were singly labeled (n = 1,912).

Topography of SON projections

The above sections establish some degree of uniformity in the output of the SON to its ipsilateral targets in NM, NA, and NL. A fundamental organizing feature of auditory systems is tonotopic organization. We sought to address whether the divergent output of SON

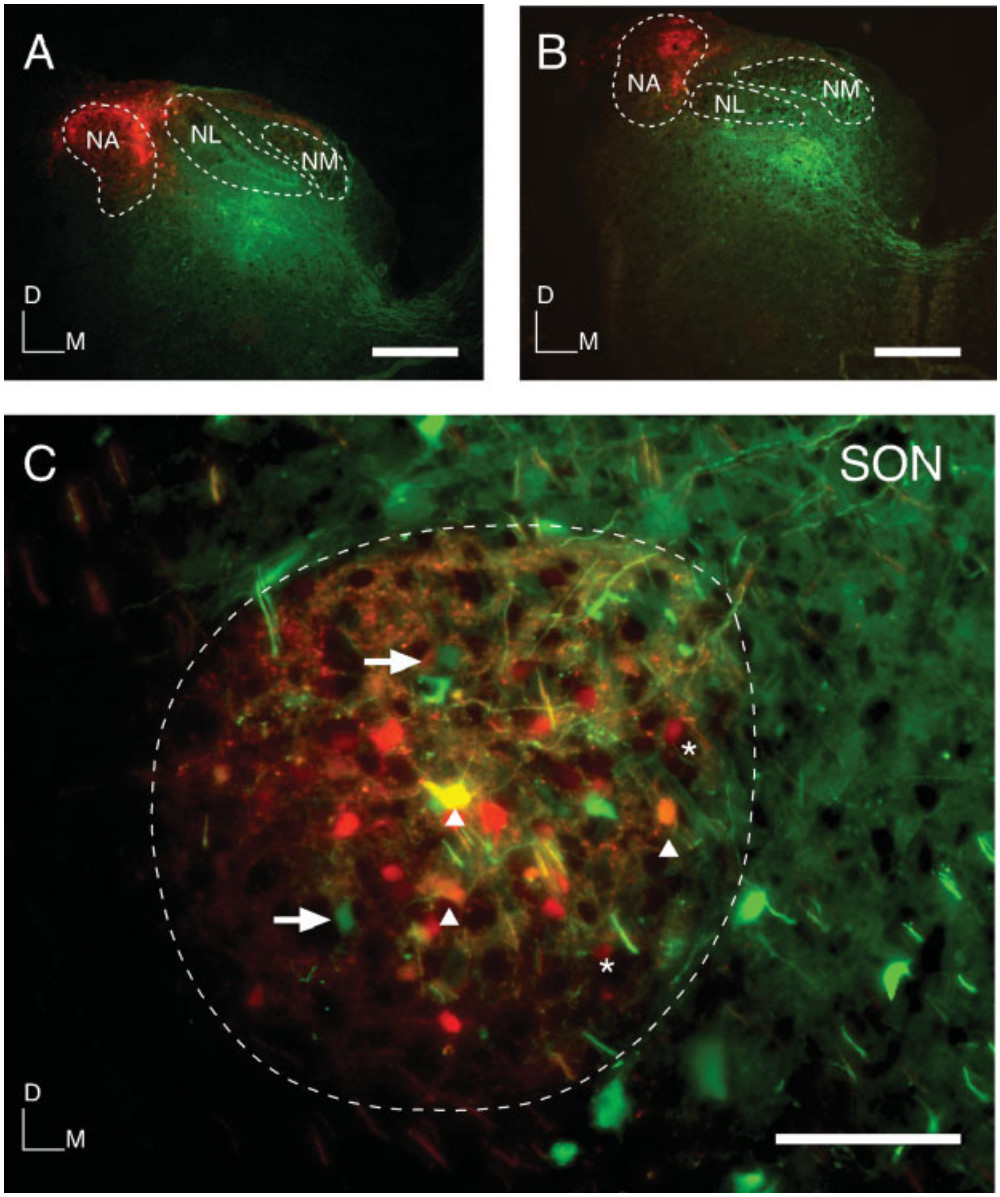

Fig. 3. Superior olivary nucleus (SON) neurons project to both nucleus angularis (NA) and nucleus laminaris (NL). **A,B:** The injection sites at rostral (A) and caudal (B) levels; nuclear borders are indicated as dotted lines. The Alexa488DA injection was centered in the ventromedial NL, and the tetramethylrhodamine dextran injection was centered in the dorsal NA. The injection sites do not overlap. NM, nucleus magnocellularis. **C:** A section through SON, where several double-labeled neurons appear (arrowheads). Singly labeled neurons are also present (arrows and asterisks). D, dorsal; M, medial. Scale bars = 500 μm in A,B; 100 μm in C.

is organized tonotopically. That is, do individual areas of SON project to restricted frequency regions of NM, NA, and NL. We exploited the fact that the best frequency of NM and NL neurons can be established precisely by their position in the nucleus (Rubel and Parks, 1975). Injection borders were recorded as percentiles between the caudal to rostral poles of the nuclei (the main tonotopic axis). In eight cases with small injections that sampled relatively small frequency regions of the tonotopic axis (mean injection = 22% of the rostrocaudal extent) in NM (n = 5) or NL (n = 3), we reconstructed the positions of labeled neurons in the SON in three dimensions from their coordinates in serial sections. To perform this analysis, we then segmented the volume of the SON by bisecting each cardinal dimension (i.e., rostrocaudal, dorsoventral, mediolateral) of the SON, yielding eight segments that we will refer to as octants. If there were a tonotopic relationship between the position of SON neurons and their projections to NM, we would expect that injection of different characteristic frequency regions of NM would yield labeled neurons that predominantly grouped in different octants of SON. Neuron number was pooled in each octant and their distributions were analyzed.

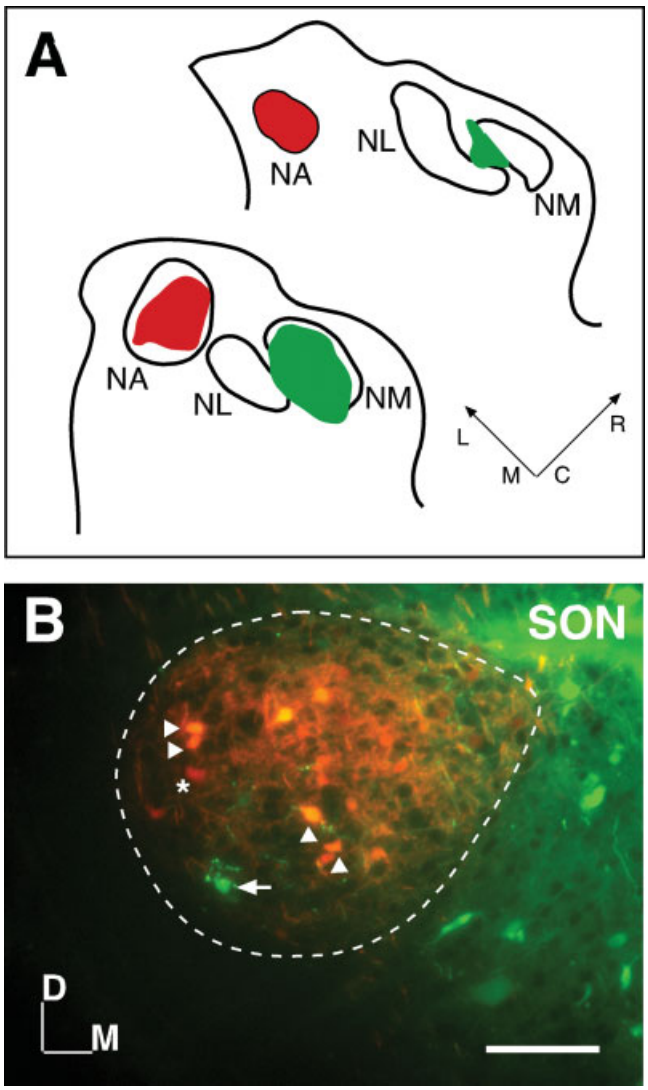

Fig. 4. Superior olivary nucleus (SON) neurons project to both nucleus angularis (NA) and nucleus magnocellularis (NM). **A:** Schematic positions of the injections along the caudal (foreground) to rostral (background) extent of the NM injection. The Alexa488DA injection also includes a small amount of dorsal nucleus laminaris (NL) neuropil. **B:** Many double-labeled SON neurons (arrowheads) as well as somata singly labeled (arrows and asterisks). L, lateral; M, medial; C, caudal; R, rostral. Scale bar = 100 μm in B.

TABLE 2. Contralateral Projection From SON Is Derived From a Separate Population of Neurons[1]

	Number of neurons		
Case	RDA contra targets	Alexa488DA ipsi targets	Double labeled
*025103d**	247	171	0
*025104f**	207	111	3
*025107d**	50	146	1
025107e	45	136	0
025109d	131	510	2
*025101e**	96	70	2
Totals	776	1144	8 (mean = 1.5%)[2]

[1]Data represent neuron counts for six preparations where contralateral and ipsilateral targets were injected with different dextrans. The number of double-labeled somata for each brain is shown in the right column. Asterisks indicate cases where contralateral injections included contralateral superior olivary nucleus. RDA, tetramethylrhodamine dextran; Alexa488DA, Alexa 488 conjugated dextran; SON, superior olivary nucleus.
[2]See Materials and Methods Section.

Figure 6A,B schematically shows two such injections and the resulting distributions of retrogradely labeled SON neurons. The case on the left shows a caudal injection that covers the 30–50th percentile of the tonotopic axis of NM, illustrated by the red zone of the vertical bar representing the full rostrocaudal extent of NM in the middle of Figure 6A. This area is predicted to represent best frequencies of roughly 0.5 to 1.5 kHz (Rubel and Parks, 1975). The SON somata distribution is shown in the two pie plots (Figure 6B, left) that represent the caudal and rostral octants. Somata are observed in all volume segments of the nucleus, but are especially prevalent in both of the dorsomedial octants. By comparison, the case shown at the right illustrates the results of a rostral injection in NM, which covers the 73–97th percentile of the rostrocaudal axis in NM and represents best frequencies of approximately 2.5 to 4.0 kHz (Rubel and Parks, 1975). This injection yielded octant counts that are surprisingly similar to those observed for the caudal injection shown to the left with the highest somata counts again in the dorsomedial octants. All five NM injections and three NL injections resulted in similar distributions of labeled somata. Thus, we did not identify a clear tonotopic organization in the SON. To validate that our injections, in fact, were restricted to a particular frequency range, we compared retrograde labeling in the well-characterized topographic projection from NM to the contralateral NL. For each of the four NL injections analyzed in this way, we observed tonotopically restricted retrograde labeling of somata in the contralateral NM. However, in each case, the labeling represented a slightly larger frequency range than that which was predicted from the borders of the injection sites. Two cases are shown in Figure 6C. Both injections labeled tonotopically restricted zones in NL. The resulting retrograde labeling yielded slightly larger but circumscribed labeling in the contralateral NM. The range of the tonotopic axis labeled in the four NMs represented 126–233% of the tonotopic axis predicted from the corresponding NL injections. These data suggest that our method of evaluating the topographic borders of our injections was to some extent conservative.

Because we did not observe any apparent tonotopic patterning in SON, we then asked whether our injections in the functionally distinct NA yielded topographically distinct labeling patterns in SON when compared with the injections in NM and NL described above. SON somata labeled from three NA injections also tended to occupy the dorsal half of SON with the highest proportion of neurons in the two dorsomedial octants (data not shown). The same patterns were present in two preparations where the topography of NA plus NM or NA plus NL injections was compared within the same animal. Thus, we did not reveal topographically distinct regions of SON from ipsilateral injections with respect to target nuclei or tonotopy within those nuclei.

Finally, we considered the possibility of differential topography between the separate populations of SON neurons that innervate either ipsilateral or contralateral targets. In all of the three cases analyzed, injections to contralateral targets yielded a pattern of somata position

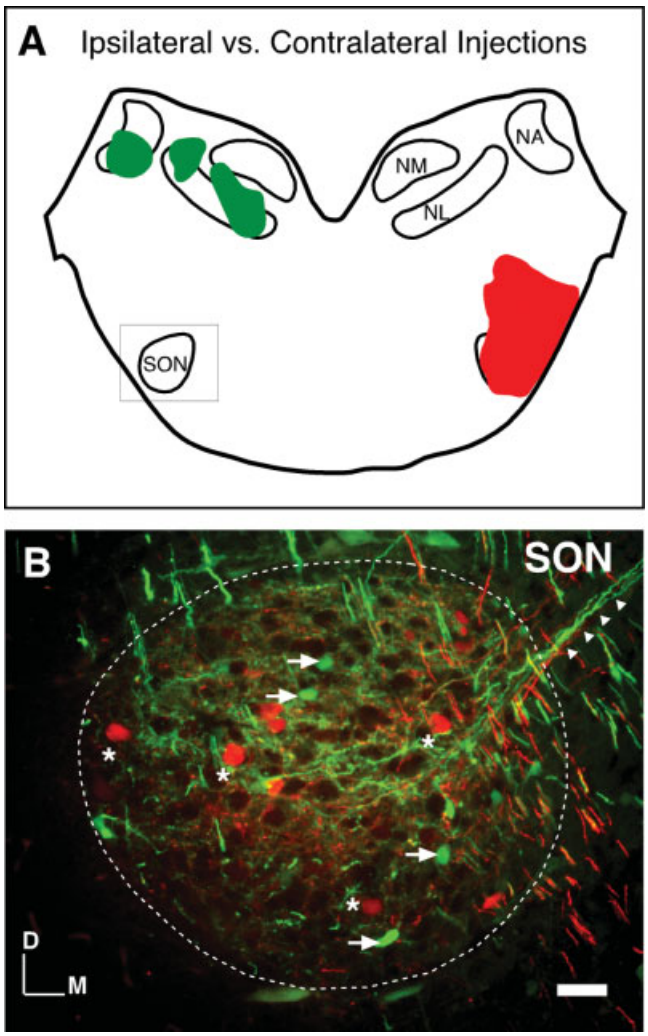

Fig. 5. Separate populations of superior olivary nucleus (SON) neurons project to ipsilateral and contralateral targets. **A:** A schematic of the brainstem with the injection sites indicated. Ipsilateral injections were primarily in nucleus angularis (NA) and nucleus laminaris (NL), but include lateral nucleus magnocellularis (NM). Contralateral injections include the rostral contralateral SON and surrounding tissue. **B:** Many singly labeled positive neurons (arrows and asterisks) but no double-labeled somata. Arrowheads show the many singly labeled fibers in the major fiber tract of the SON. Scale bar = 100 μm in B.

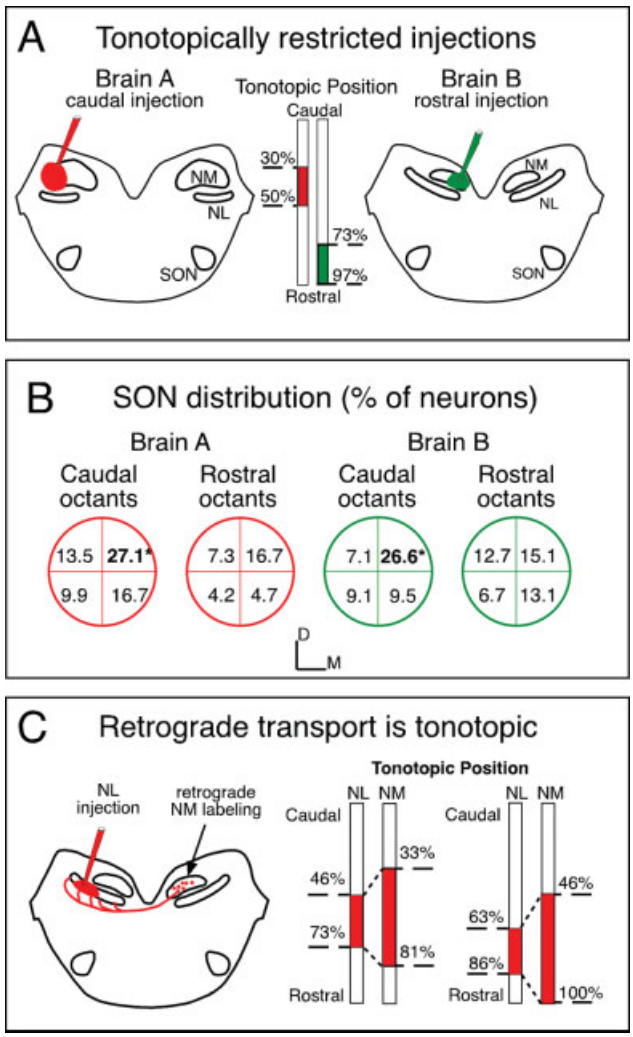

Fig. 6. Topography of superior olivary nucleus (SON) is not organized strictly according to best frequency. **A:** Schematic projections of two preparations with injections that span restricted best frequency domains in nucleus magnocellularis (NM). Brain A shows a caudal injection red, whereas brain B shows a rostral injection green. The vertical bars in the middle of the panel provide a comparison of the injection sites along the tonotopic axis. **B:** The percentage distribution of neurons counted in the eight approximately equal volume segments (octants) of the SON. Neurons are distributed throughout the SON in both cases. However, for both the low frequency (red circles) and high frequency (green circles) injections, SON somata are concentrated in the dorsomedial segments. The octant with the highest proportion of neurons is the same in both cases and is marked in bold and by asterisks. **C:** Tonotopically restricted injections in nucleus laminaris (NL) result in tonotopically restricted labeling in the contralateral NM. The schematic brain panel at left illustrates the experiment. The vertical bars to the right show the results of two experiments. In both cases, there was perfectly tonotopic, although expanded, retrograde labeling of contralateral NM neurons.

strikingly different than the ipsilaterally labeled neurons. Neurons labeled from the ipsilateral targets yielded the same pattern as those presented above. Somata were distributed throughout the nucleus but with the population most concentrated in the dorsomedial octant volumes of SON. In contrast, the contralateral injections also labeled neurons throughout the nucleus, but somata occurred most frequently in the ventrolateral octants of SON. The data from these three cases were pooled and are presented in Figure 7. In Figure 7A, we show the average neuron percentage counts from ipsilateral (Figure 7A, green circle at left) and contralateral (Figure 7A, red circle at right) injections for each octant. These data indicate that SON is topographically organized, at least in part, according to the origin of its contralateral and ipsilateral projections. A Chi-squared analysis showed the differential distributions of labeled somata as a function of ipsilateral or contralateral injection of tracer to be statistically significant, $P \leq 0.001$. Figure 7B shows a schematic drawing of the SON projections that incorporates the results presented in this

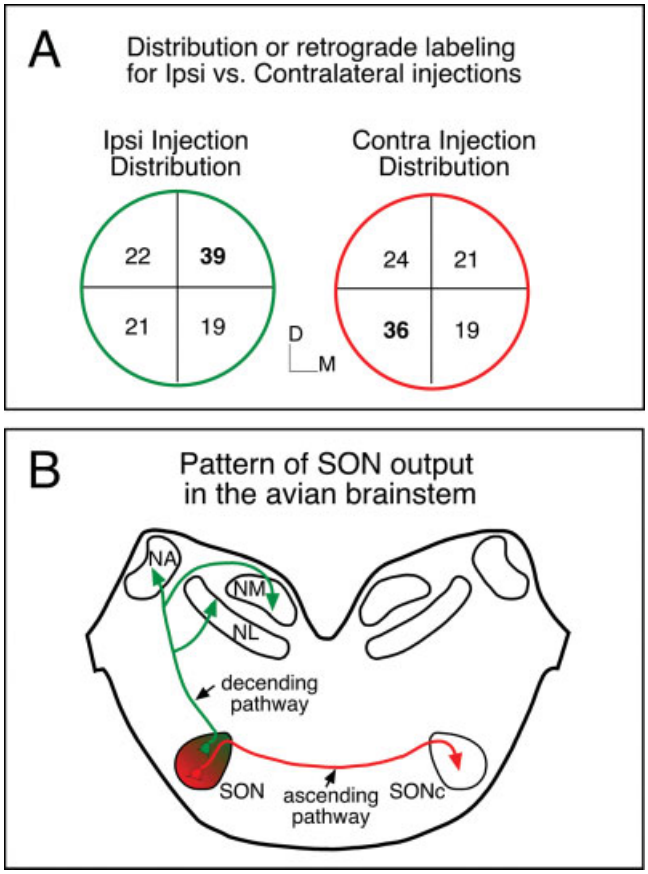

Fig. 7. Superior olivary nucleus (SON) topography is organized according to postsynaptic targets. **A:** Average percentage distributions from three preparations where the contralateral and ipsilateral targets were labeled with different fluorophores. The data from the rostral and caudal octants are combined for clarity. The green circle at left shows the distribution of neurons labeled from ipsilateral injections. Consistent with the data shown in Figure 6, retrogradely labeled SON neurons were most frequent in the dorsomedial SON marked in bold. The red circle at the right shows the pooled distribution resulting from three contralateral injections. Neurons are again widely distributed in SON but concentrated in the ventrolateral SON (marked in bold). A Chi-square analysis showed the differential distributions of somata to be statistically significant, $P \leq 0.001$. D, dorsal; M, medial. **B:** A schematic summary of all results, including the projection pattern and topographic organization of SON. Ipsilateral projections arise from the dorsomedial SON (green lines) and independent contralateral projections (red line) project from the ventrolateral SON to the contralateral SON (SONc). NA, nucleus angularis; NM, nucleus magnocellularis; NL, nucleus laminaris.

report. The ipsilateral projection (Figure 7B, green) originates primarily in the dorsomedial SON with single neurons innervating multiple targets in NA, NM, and NL. The contralateral projection (Figure 7B, red) originates from a separate population of neurons that reside predominantly in the ventrolateral SON.

DISCUSSION

These data support two main conclusions. First, the topography of the SON is organized according to functionally distinct output projections (ipsilateral and contralateral) that arise from separate populations of neurons. Second, SON neurons provide divergent feedback to multiple targets in the ipsilateral brainstem, often innervating multiple anatomically and functionally distinct targets and displaying no obvious tonotopy. In this section, we briefly expand upon these findings and present a conceptual model of inhibitory function in ITD processing that incorporates these results.

Topography

Injections into tonotopically restricted regions of NM or NL yielded no distinct patterning of labeled somata in SON. In contrast, reliable tonotopic labeling in the contralateral NM was seen after tonotopically restricted NL injections. Although some expansion along the frequency axis in NM relative to the NL injection sites suggests that our methods may not resolve a coarsely organized tonotopy in the SON projection, it is reasonable to conclude that this efferent projection must be quite diffuse compared with other known projections to NM, NA, or NL. Moiseff and Konishi, (1983) reported a rough dorsal to ventral tonotopic gradient in electrophysiological responses in SON of the barn owl, but no data were presented. Therefore, a viable hypothesis at this time is that tonotopically organized input axons activate inhibitory feedback that operates broadly across the frequency axes of the ipsilateral target nuclei.

This finding is in contrast to the precise tonotopy shown in other avian brainstem connections as well as in most mammalian auditory pathways. This arrangement is surprising in light of the elegant tonotopic architecture of neurons in one of SONs primary targets, NL (Smith and Rubel, 1979). On the other hand, if one of the primary functions of the ipsilateral SON recurrent circuitry is to adjust ongoing or spontaneous firing rates such that a signal will have maximal influence, then a broadly dispersed nontonotopic input would be advantageous. This function would be most important in conditions of high noise levels where sounds would activate large areas of the cochlea even when the background noise has a limited bandwidth.

Separation of ipsilateral and contralateral projections

Preparations in which ipsilateral and contralateral targets were differentially labeled yielded exceedingly small numbers of double-labeled neurons in SON. The presence of two separate SON outputs is supported by the differential topographic distributions of ipsilaterally and contralaterally labeled somata. It remains unresolved whether this contralateral output is solely GABAergic. However, (Lachica et al., 1994) reported that more than 70% of SON neurons were immunoreactive for GABA. Moreover, while the contralateral SON projection is biased toward the ventrolateral region of SON, no such bias was seen in studies of GABA immunoreactivity within the nucleus. Because we often labeled hundreds of contralaterally projecting neurons, it is likely that this projection is at least in part GABAergic.

Our most surprising result is that single SON neurons commonly project to multiple, functionally distinct ipsilateral targets. Hence, functionally distinct parallel pathways established by NM and NA are bound together in the brainstem by common inhibitory feedback projections. Previous studies in both barn owl and chicken reported

that the NL projection to SON is biased toward the dorsal SON (Conlee and Parks, 1986; Takahashi and Konishi, 1988), while the NA innervates primarily the ventral SON. Taken together with the current results, these data suggest that the SON is organized according to two functional zones; a dorsomedial region provides feedback inhibition to multiple ipsilateral targets, and a ventrolateral zone projects to contralateral targets. A rationale for this division of output projections is suggested below.

Functional significance

Previous studies have led to two main conclusions about the SON's role in auditory function. First, several previous studies have suggested that inhibitory input to both NM and NL in the "timing pathway" serves to increase the acuity of temporal integration by minimizing temporal summation on the plasma membrane. The shortening of the membrane time constant is achieved by a depolarizing GABAergic conductance that activates low voltage activated potassium (K^+_{LVA}) conductances. Large K^+_{LVA} conductances are a common feature of neurons specialized for encoding temporal features of sounds, and a protein subunit of these channel types Kv1.1 is highly expressed in NM and NL neurons (Lu et al., 2004). Thus, inhibitory input likely results in improved coincidence detection in NL and phase-locking to the stimulus waveform in both NM and NL (Reyes et al., 1996; Funabiki et al., 1998; Yang et al., 1999; Monsivais et al., 2000).

The coupling of the GABAergic input to the K^+_{LVA} conductance as well as the prominent asynchronous release observed at these synapses (Lu and Trussell, 2000; Monsivais and Rubel, 2001), results in temporally expanded inhibitory events. The long kinetics suggest that the inhibition in the avian auditory brainstem operates on a time scale relevant only to general changes in sound level and will not provide transient or cycle-by-cycle feedback. Therefore, the convergence of direct and indirect (by means of NM) inputs to NL from SON predicted by divergent axon collaterals observed in this study will have little differential influence on temporal aspects of inhibitory input.

A second proposed role for the inhibitory feedback is the suppression of discharges in its targets over a broad range of sound intensities. This role would result in an expansion of the dynamic range of neurons in these nuclei. This proposed "gain control" mechanism acting on NM and NL neurons has been suggested to preserve ITD coding over a broad range of intensities in NL (Pena et al., 1996; Funabiki et al., 1998; Yang et al., 1999; Lu and Trussell, 2000). The role of inhibition in NA has not been directly tested. However, the diversity of physiological response types observed in NA provides ample substrate for inhibition to influence both basic response characteristics and rate-level functions (Hotta, 1971; Sachs and Sinnott, 1978; Sullivan and Konishi, 1984; Warchol and Dallos, 1990; Soares et al., 2002; Köppl and Carr, 2003).

From the present study, a new perspective on inhibition in the auditory brainstem emerges, consisting of two separate inhibitory feedback loops, each providing generalized and divergent inhibition of the major auditory centers in the ipsilateral brainstem. These parallel feedback circuits are then coupled by an independent reciprocal inhibition. The importance of the data presented here is twofold. First, the merging of parallel pathways ipsilaterally provides the circuitry for the SON to regulate its impact on both monaural cochlear nuclei in the absence of direct projections from NM. In other words, the circuitry allows for the inhibitory input to NM to be regulated by "proxy" through the coupled parallel reciprocal feedback between NA and SON. Second, a separate contralateral pathway originates from a region of SON that receives input primarily from the monaural NA. This arrangement may allow each SON to influence the other proportionally to the input strength at each ear, without the confounding influence of binaural inputs from NL. Taken together, these data on SON circuitry necessitate a revised view of inhibitory function in binaural processing and suggest that the robust reciprocal connections between the SONs contribute to ITD processing in NL.

Our rationale for this view relies on three well-documented features of the avian auditory system. First, whereas binaural coincidence results in maximal firing rates in NL, these neurons respond well to monaural stimuli in a level-dependent manner in both barn owl and chicken (Overholt et al., 1992; Joseph and Hyson, 1993; Pena et al., 1996). Second, NM neurons, the sole excitatory input to NL, show up to a fivefold increase in firing rate over an intensity range of only approximately 20 dB (Sachs and Sinnott, 1978; Warchol and Dallos, 1990). Third, the air-filled canal that couples the middle ears of birds expands the range of ITDs at low frequencies beyond that which is predicted by the distance between the two ears and also induces de facto interaural intensity differences (IIDs) by biasing the tympanic membranes (Coles et al., 1980; Hill et al., 1980; Rosowski and Saunders, 1980; Calford and Piddington, 1988; Hyson et al., 1994). By using cochlear microphonic recordings, Hyson et al. (1994) showed that IID in chicks changed systematically with sound source location. These changes are robust and similar across frequency. These IIDs may be as large as 6–10 dB and, thus, could result in large differences in firing rates between the two NMs. This bilateral asymmetry in firing rates generates a computational challenge for NL; put simply, an NL neuron must have a mechanism to distinguish between an intense monaural input and ideally timed binaural inputs.

In Figure 8, we present a conceptual model focusing on a systems level mechanism of binaural intensity compensation that incorporates the known circuitry of the SON. Recent computational modeling of this system supports this view (Dasika, 2003). The reader will note that the temporal and/or gain control contribution of the SON to response properties of NA and NL neurons, although fundamental aspects of the SON output, are not included in the presentation of this model to highlight specifically the SONs' influence on input biases to NL.

Each panel of Figure 8 represents a single NL and its bilateral inputs from the two NMs. Notice that the left NM projects with similar axon lengths on the "ipsilateral" side, whereas the length of the right NM axon increases from top to bottom resulting in the well-known delay line present in the chicken (Young and Rubel, 1983; Overholt et al., 1992). Figure 8A shows expected neuronal responses to the idealized conditions in which sounds generate no differences in input strength, just ITDs. This finding is represented by the speaker positioned on the midline, the only actual location for which there are no input level biases. Because there are no IIDs and, thus, no imbalance in input strength to NL, the circuitry involving SON is equally stimulated on both sides of the brain and

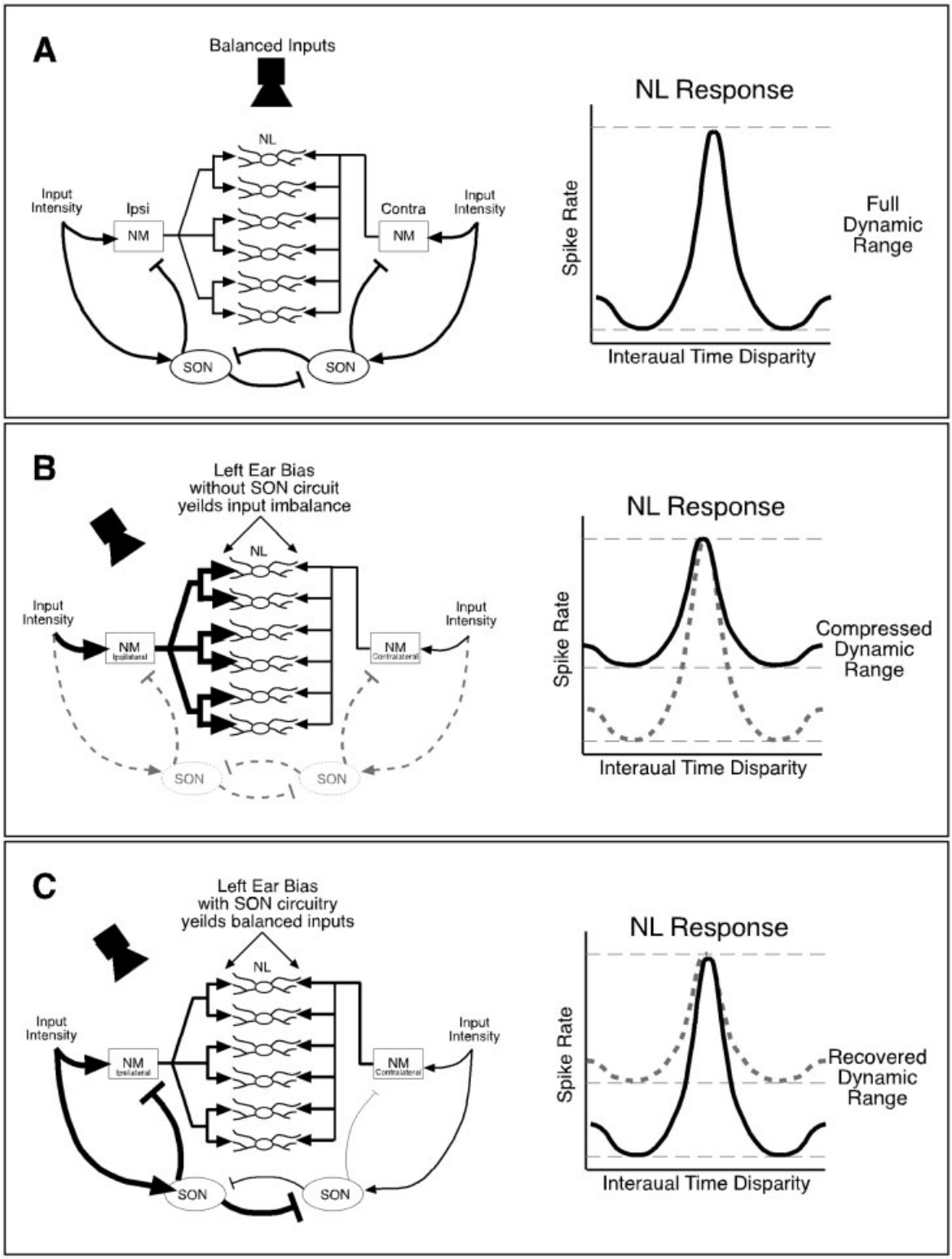
A
Balanced Inputs
NL
Input Intensity
Ipsi
NM
Contra
NM
Input Intensity
SON
SON
NL Response
Spike Rate
Full Dynamic Range
Interaual Time Disparity
B
Left Ear Bias without SON circuit yeilds input imbalance
NL
Input Intensity
NM Ipsilateral
NM Contralateral
Input Intensity
SON
SON
NL Response
Spike Rate
Compressed Dynamic Range
Interaual Time Disparity
C
Left Ear Bias with SON circuitry yeilds balanced inputs
NL
Input Intensity
NM Ipsilateral
NM Contralateral
Input Intensity
SON
SON
NL Response
Spike Rate
Recovered Dynamic Range
Interaual Time Disparity

Figure 8

the reciprocal connection between the SONs is mutually canceled, leaving only equivalent bilateral feedback inhibition and a fully modulated change in firing rate with ITD.

Figure 8B illustrates an intensity imbalanced input represented by a lateralized speaker in the absence of SON circuitry. The lateralized sound source causes a shift in ITD, but also generates an IID through interaural coupling. The relatively high activity in the left NM compared with the NM on the right causes its input to dominate at NL. All NL neurons increase their firing rates relative to the strong monaural input to the left ear regardless of the binaural timing characteristics of the signal. In the response shown to the right of Figure 8B, the dynamic range of NL neurons becomes compressed and the relative change in firing rate from best to worst ITD is reduced. In other words, in the absence of compensation for binaural intensity differences, the influence of the ITD on the firing in NL is reduced because the system is asymmetrically driven by a binaural intensity difference.

Figure 8C shows the same sound presentation, but with the SON circuit intact. The increased intensity to the left ear has several effects on firing in the two NMs: (1) it tends to drive higher firing rates in the left NM relative to its contralateral counterpart; (2) it recruits a strong inhibition from the left SON back to the ipsilateral NM, reducing its firing rate; and (3) the ipsilateral (left) SON suppresses the SONc, resulting in a disinhibition of the contralateral (right) NM. This coupling of the SONs causes an increased firing rate in the contralateral NM, while simultaneously decreasing the ipsilateral NM firing rate. In this way, shifts in IID will be dynamically counterbalanced by this circuit as sound sources shift position. In summary, we propose that the binaural coupling of the SON circuitry is ideally suited to eliminate confounding of ITD cues by counterbalancing IIDs and, thus, preserve spatial coding in NL.

Fig. 8. Conceptual model of superior olivary nucleus (SON) function in binaural processing. Each panel at left shows schematic brainstem circuits, including a single nucleus laminaris (NL), as well as its inputs from both nucleus magnocellulari (NMs), and SONs. The NM input from the left innervates all NL neurons with the same delay, whereas the input from the right NM innervates NL with increasing delays from top to bottom. Input strength to each nucleus is represented by line weight, with heavy lines indicating strong input. Excitatory inputs are shown with arrowheads and inhibitory inputs are shown with T-bars. At right, each panel shows the expected response of a representative NL neuron at that neuron's best delay in black. In each case, the neurons' best interaural time difference (ITD) is centered on the X axis. **A:** The circuit's response to a midline sound presentation. In this case, NL neurons are presented with matched inputs from either side that only differ in arrival time according to the delay line on the right, and the NL neuron response is modulated over its full dynamic range as ITD varies. **B:** A sound source that is shifted toward the left ear with the SON circuitry disconnected. In this case, the NM at left is driven to higher firing rates than the right NM. This finding results in strong input to all NL cells that is unrelated to the relative timing between the two ears. A smaller modulation in firing rate results from coincident input from the contralateral ear at the best ITD. The original ITD plot is shown with gray dotted lines. **C:** The same stimulus conditions as those in B, but with the SON circuitry intact. This inhibition reduces the input strength to NL from the ipsilateral ear. At the same time, the ipsilateral SON inhibits its contralateral counterpart, which in turn releases the contralateral NM from inhibition. In this way, the intensity bias at the tympanic membranes is offset by the inhibition of the left NM and disinhibition of the right NM. As a result of the cancellation of intensity differences in the circuit, the only input cue to NL that varies with sound source location is ITD.

Comparison to mammals

The feedback of the SON to cochlear nuclei (CN) bears intriguing similarities to the circuitry of some periolivary nuclei in mammals. All subdivisions of the mammalian CN receive glycinergic and GABAergic input from periolivary regions, in particular, the contralateral ventral nucleus of the trapezoid body, the ipsilateral medial nucleus of the trapezoid body, and lateral nucleus of the trapezoid body (Adams, 1983; Spangler et al., 1987; Schofield, 1994; Warr and Beck, 1996; Ostapoff et al., 1997). Physiological studies have demonstrated inhibitory modification of responses in several classes of mammalian CN neurons (Caspary et al., 1994; Ebert and Ostwald, 1995a,b; Backoff et al., 1999; Kopp-Scheinpflug et al., 2002). Additionally, the nature of the feedback suggests that olivary projections to the CN may have a similar role to that proposed for SON in binaural processing (Schofield, 1994). The similarities between avian and mammalian circuitry and the simplicity of this circuit in birds make the avian system an attractive model for further investigation of inhibitory feedback in vertebrate auditory systems.

ACKNOWLEDGMENTS

We thank Dr. Jialin Shang, Dale Cunningham, and Glen MacDonald for their dedication and ongoing contributions to this research. Additionally, we also thank Drs. George D. Pollak and Brett Schofield for their helpful comments on earlier versions of this article.

LITERATURE CITED

Adams JC. 1983. Cytology of periolivary cells and the organization of their projections in the cat. J Comp Neurol 215:275–289.

Backoff PM, Shadduck Palombi P, Caspary DM. 1999. Gamma-aminobutyric acidergic and glycinergic inputs shape coding of amplitude modulation in the chinchilla cochlear nucleus. Hear Res 134:77–88.

Boord RL, Rasmussen GL. 1963. Projection of the cochlear and lagenar nerves on the cochlear nuclei of the pigeon. J Comp Neurol 120:463–475.

Calford MB, Piddington RW. 1988. Avian interaural canal enhances interaural delay. J Comp Physiol [A] 162:503–510.

Carr CE, Konishi M. 1990. A circuit for detection of interaural time differences in the brain stem of the barn owl. J Neurosci 10:3227–3246.

Carr CE, Fujita I, Konishi M. 1989. Distribution of GABAergic neurons and terminals in the auditory system of the barn owl. J Comp Neurol 286:190–207.

Caspary DM, Backoff PM, Finlayson PG, Palombi PS. 1994. Inhibitory inputs modulate discharge rate within frequency receptive fields of anteroventral cochlear nucleus neurons. J Neurophysiol 72:2124–2133.

Coles RB, Lewis DB, Hill KG, Hutchings ME, Gower DM. 1980. Directional hearing in the Japanese quail (Coturnix-Coturnix-Japonica). II. Cochlear physiology. J Exp Biol 86:153–170.

Conlee JW, Parks TN. 1986. Origin of ascending auditory projections to the nucleus mesencephalicus lateralis pars dorsalis in the chicken. Brain Res 367:96–113.

Correia MJ, Eden AR, Westlund KN, Coulter JD. 1982. Organization of ascending auditory pathways in the pigeon (Columba livia) as determined by autoradiographic methods. Brain Res 234:205–212.

Dasika VK. 2003. Models of auditory brainstem coincidence-detector neurons. Boston: Boston College of Engineering. p 1–194.

Ebert U, Ostwald J. 1995a. GABA alters the discharge pattern of chopper neurons in the rat ventral cochlear nucleus. Hear Res 91:160–166.

Ebert U, Ostwald J. 1995b. GABA can improve acoustic contrast in the rat ventral cochlear nucleus. Exp Brain Res 104:310–322.

Funabiki K, Koyano K, Ohmori H. 1998. The role of GABAergic inputs for coincidence detection in the neurones of nucleus laminaris of the chick. J Physiol 508(Pt 3):851–869.

Haas K, Jensen K, Sin WC, Foa L, Cline HT. 2002. Targeted electroporation in Xenopus tadpoles in vivo- from single cells to the entire brain. Differentiation 70:148–154.

Hackett JT, Jackson H, Rubel EW. 1982. Synaptic excitation of the second and third order auditory neurons in the avian brain stem. Neuroscience 7:1455–1469.

Hill KG, Lewis DB, Hutchings ME, Coles RB. 1980. Directional hearing in the Japanese quail (Coturnix-Coturnix-Japonica). I. Acoustic properties of the auditory-system. J Exp Biol 86:135–151.

Hotta T. 1971. Unit responses from the nucleus angularis in the pigeon's medulla. Comp Biochem Physiol A 40:415–424.

Hyson RL, Overholt EM, Lippe WR. 1994. Cochlear microphonic measurements of interaural time differences in the chick. Hear Res 81:109–118.

Joseph AW, Hyson RL. 1993. Coincidence detection by binaural neurons in the chick brain stem. J Neurophysiol 69:1197–1211.

Kopp-Scheinpflug C, Dehmel S, Dorrscheidt GJ, Rubsamen R. 2002. Interaction of excitation and inhibition in anteroventral cochlear nucleus neurons that receive large endbulb synaptic endings. J Neurosci 22: 11004–11018.

Köppl C. 1997. Phase locking to high frequencies in the auditory nerve and cochlear nucleus magnocellularis of the barn owl, Tyto alba. J Neurosci 17:3312–3321.

Köppl C, Carr CE. 2003. Computational diversity in the cochlear nucleus angularis of the barn owl. J Neurophysiol 89:2313–2329.

Lachica EA, Rubsamen R, Rubel EW. 1994. GABAergic terminals in nucleus magnocellularis and laminaris originate from the superior olivary nucleus. J Comp Neurol 348:403–418.

Lu T, Trussell LO. 2000. Inhibitory transmission mediated by asynchronous transmitter release. Neuron 26:683–694.

Lu T, Trussell LO. 2001. Mixed excitatory and inhibitory GABA-mediated transmission in chick cochlear nucleus. J Physiol 535:125–131.

Lu Y, Monsivais P, Tempel BL, Rubel EW. 2004. Activity-dependent regulation of the potassium channel subunits Kv1.1 and Kv3.1. J Comp Neurol 470:93–106.

Moiseff A, Konishi M. 1983. Binaural characteristics of units in the owls brain-stem auditory pathway: precursors of restricted spatial receptive-fields. J Neurosci 3:2553–2562.

Monsivais P, Rubel EW. 2001. Accommodation enhances depolarizing inhibition in central neurons. J Neurosci 21:7823–7830.

Monsivais P, Yang L, Rubel EW. 2000. GABAergic inhibition in nucleus magnocellularis: implications for phase locking in the avian auditory brainstem. J Neurosci 20:2954–2963.

Neumann E, Kakorin S, Toensing K. 1999. Fundamentals of electroporative delivery of drugs and genes. Bioelectrochem Bioenerg 48:3–16.

Ostapoff EM, Benson CG, Saint Marie RL. 1997. GABA- and glycine-immunoreactive projections from the superior olivary complex to the cochlear nucleus in guinea pig. J Comp Neurol 381:500–512.

Overholt EM, Rubel EW, Hyson RL. 1992. A circuit for coding interaural time differences in the chick brainstem. J Neurosci 12:1698–1708.

Parks TN, Rubel EW. 1975. Organization and development of brain stem auditory nuclei of the chicken: organization of projections from n. magnocellularis to n. laminaris. J Comp Neurol 164:435–448.

Parks TN, Rubel EW. 1978. Organization and development of the brainstem auditory nuclei of the chicken: primary afferent projections. J Comp Neurol 180:439–448.

Pena JL, Viete S, Albeck Y, Konishi M. 1996. Tolerance to sound intensity of binaural coincidence detection in the nucleus laminaris of the owl. J Neurosci 16:7046–7054.

Ramon y Cajal S. 1971. The acoustic nerve: its cochlear branch or cochlear nerve.

Rámon y Cajal S. 1908 Les ganglions terminaux du nerf acoustique des oiseaux. Trab Inst Cajal Invest Biol 6:195–225.

Reyes AD, Rubel EW, Spain WJ. 1996. In vitro analysis of optimal stimuli for phase-locking and time-delayed modulation of firing in avian nucleus laminaris neurons. J Neurosci 16:993–1007.

Rosowski JJ, Saunders JC. 1980. Sound-transmission through the avian inter-aural pathways. J Comp Physiol 136:183–190.

Rubel EW. 1978. Ontogeny of structure and function in the vertebrate auditory system. In: Jacobson M, editor. Handbook of sensory physiology. Berlin: Springer-Verlag. p 135–237.

Rubel EW, Parks TN. 1975. Organization and development of brain stem auditory nuclei of the chicken: tonotopic organization of n. magnocellularis and n. laminaris. J Comp Neurol 164:411–433.

Sachs MB, Sinnott JM. 1978. Responses to tones of single cells in nucleus magnocellularis and nucleus angularis of Redwing Blackbird (Agelaius-Phoeniceus). J Comp Physiol 126:347–361.

Schofield BR. 1994. Projections to the cochlear nuclei from principal cells in the medial nucleus of the trapezoid body in guinea pigs. J Comp Neurol 344:83–100.

Smith DJ, Rubel EW. 1979. Organization and development of brain stem auditory nuclei of the chicken: dendritic gradients in nucleus laminaris. J Comp Neurol 186:213–239.

Soares D, Carr CE. 2001. The cytoarchitecture of the nucleus angularis of the barn owl (Tyto alba). J Comp Neurol 429:192–205.

Soares D, Chitwood RA, Hyson RL, Carr CE. 2002. Intrinsic neuronal properties of the chick nucleus angularis. J Neurophysiol 88:152–162.

Spangler KM, Cant NB, Henkel CK, Farley GR, Warr WB. 1987. Descending projections from the superior olivary complex to the cochlear nucleus of the cat. J Comp Neurol 259:452–465.

Sullivan WE, Konishi M. 1984. Segregation of stimulus phase and intensity coding in the cochlear nucleus of the barn owl. J Neurosci 4:1787–1799.

Takahashi TT, Konishi M. 1988. Projections of nucleus angularis and nucleus laminaris to the lateral lemniscal nuclear complex of the barn owl. J Comp Neurol 274:212–238.

Trussell LO. 1999. Synaptic mechanisms for coding timing in auditory neurons. Annu Rev Physiol 61:477–496.

Viete S, Pena JL, Konishi M. 1997. Effects of interaural intensity difference on the processing of interaural time difference in the owl's nucleus laminaris. J Neurosci 17:1815–1824.

von Bartheld CS, Rubel EW. 1989. Transient GABA immunoreactivity in cranial nerves of the chick embryo. J Comp Neurol 286:456–471.

Warchol ME, Dallos P. 1990. Neural coding in the chick cochlear nucleus. J Comp Physiol [A] 166:721–734.

Warr WB, Beck JE. 1996. Multiple projections from the ventral nucleus of the trapezoid body in the rat. Hear Res 93:83–101.

Westerberg BD, Schwarz DW. 1995. Connections of the superior olive in the chicken. J Otolaryngol 24:20–30.

Yang L, Monsivais P, Rubel EW. 1999. The superior olivary nucleus and its influence on nucleus laminaris: a source of inhibitory feedback for coincidence detection in the avian auditory brainstem. J Neurosci 19:2313–2325.

Young SR, Rubel EW. 1983. Frequency-specific projections of individual neurons in chick brainstem auditory nuclei. J Neurosci 3:1373–1378.